Differential, state-to-state, and total-charge-transfer cross sections for H^+ colliding with Ar

R. Cabrera-Trujillo, A. Amaya-Tapia, and A. Antillón
Instituto de Ciencias Físicas, Universidad Nacional Autónoma de México, Apartado Postal 48-3, Cuernavaca, Morelos, 62251, Mexico
(Received 14 July 2008; revised manuscript received 23 October 2008; published 26 January 2009)

Differential, direct, state-to-state, and summed charge-transfer cross sections in collisions of protons with argon atoms have been studied at collision energies ranging from 10 eV to 100 keV by means of two different methods: a semiclassical coupled-channel and a nonadiabatic electron-nuclear dynamics approach. Our results for the direct differential cross section show excellent agreement between theory and the available experimental data. We discuss the effect of the interference in the differential cross sections caused by different projectile trajectories that have the same scattering angle. A comparison of the methods shows that the repulsive and attractive parts of the interaction potential are required in the trajectory dynamics for the correct description of the deflection of the projectile and the electron capture probability at the low-intermediate energies and intermediate to low impact parameter region. For energies greater than ~4 keV, the theoretical methods follow the trend of the experimental data. We find that the $2s$, $2p$, and total cross sections change about three orders of magnitude for energies below 1 keV down to 0.01 keV. We also find that the electron capture probability into the $1s$ orbital as a function of the projectile energy and impact parameter forms a ridge that extends toward the high impact parameter region and low projectile energies.

DOI: 10.1103/PhysRevA.79.012712 PACS number(s): 34.70.+e, 34.50.−s

I. INTRODUCTION

Electron transfer processes in collisions of heavy ions with a variety of target materials at various projectile energies is important in a number of applications that range from plasma diagnostic [1] to atmospheric science [2], radiobiology, and tumor therapy [3].

In the case of protons colliding with argon atoms, the electron capture occurs mainly in the $n=1$ state of hydrogen with a small contribution from the low excited states of hydrogen. For the case of a many-electron system, the theoretical description turns out to be very demanding. The main problem is the correlation of the electron-electron interaction, which prohibits the factorization of the many-electron wave function into several one-electron states. This effect makes the theoretical treatment of any multielectron system very time-consuming.

Previous calculations by Amaya-Tapia *et al.* [4] and Kirchner *et al.* [5] provided a first detailed comparison between theory and experiment for total and state-to-state capture cross sections. Both approaches are based on time-dependent independent-particle models. The work of Kirchner *et al.* is built upon the stationary optimized potential method (OPM) of density-functional theory (DFT) with response. Hereafter, we refer to the work of Kirchner as OPM-DFT. In the work of Amaya-Tapia, the coupled-channel (CC) independent-particle method [6,7] was employed. Both of these methods are based on one active electron for the description of the transitions and require a statistical analysis for the impact-parameter-dependent electronic capture probabilities. In the OPM-DFT work, it was found that electronic response is necessary for a proper description of the electron capture process.

In order to overcome these approximations, the same system is studied in this work with an approach that takes into account the many-electron character of the system, as well as the incorporation of full nonadiabatic dynamics. Furthermore, the previous CC results of Ref. [4] are recalculated with a better optimization of the wave function and an improved statistical analysis model.

Thus, in this paper, we address the direct and charge exchange differential, total, and state-to-state electron capture cross section for protons colliding with argon atoms. We have extended the projectile energies from 10 eV up to 100 keV by means of a nonadiabatic, full coupled electron-nuclear dynamics that takes into account the dynamic response of the electrons and nuclei. The CC calculations are reported for energies larger than 1 keV. In order to estimate the contribution of a many-electron system to the cross section, a comparison between these two approaches is made. The paper is arranged in the following form. Section II provides an overview of the theoretical approach and computational implementation of our methods. Section III A presents our results for the impact parameter dependence of the electron capture probability, followed, in Sec. III B, by the direct and charge exchange differential cross section. In Sec. III C, the total electron transfer cross section and the state-to-state electron capture cross section are analyzed. Finally, in Sec. IV our conclusions are presented.

II. THEORETICAL AND COMPUTATIONAL APPROACH

A. Electron-nuclear dynamics method

The electron-nuclear dynamics (END) method is an *ab initio*, explicitly time-dependent theory that accounts for nonadiabatic effects when solving the Schrödinger equation of the system. In its simplest form, it is based on a system state vector $|\psi(t)\rangle=|R(t),P(t)\rangle|z(t),R(t),P(t)\rangle$. The ket $|R(t),P(t)\rangle$ is the nuclear wave function, which is a product of traveling Gaussians representing distinguishable nuclei with average positions, $\mathbf{R}_k$, and momenta, $\mathbf{P}_k$. The ket $|z(t),R(t),P(t)\rangle$ represents the electron wave function, which in configuration space is given by a Thouless determinant [8]

$\langle x|z(t),R(t),P(t)\rangle=\det\{\chi_i(\mathbf{x}_j)\}$ of complex nonorthogonal spin orbitals $\chi_h=u_h+\Sigma_p z_{ph}u_p$ in terms of a basis, u_i, represented as a linear combination of atomic orbitals (LCAO) of Gaussian basis set centered on the average nuclear positions $\mathbf{R}_k$ and traveling with momenta $\mathbf{P}_k$, i.e., it includes electron translation factors.

Application of the time-dependent variational principle to the action produced by the quantum-mechanical Lagrangian $L=\langle\psi|i\hbar\partial/\partial t-H|\psi\rangle/\langle\psi|\psi\rangle$ results in Euler-Lagrange equations that are the variational approximation to the time-dependent Schrödinger equation. The complex Thouless coefficients z_{ph} and the Cartesian components of the average nuclear positions $\mathbf{R}_k$ and momenta $\mathbf{P}_k$ play the role of dynamical variables. In the narrow width limit for the nuclear wave packets, the equations that govern the time evolution of the dynamical variables are expressed in matrix form as

$$\begin{bmatrix} i\mathbf{C} & \mathbf{0} & i\mathbf{C}_\mathbf{R} & i\mathbf{C}_\mathbf{P} \\ \mathbf{0} & -i\mathbf{C}^* & -i\mathbf{C}_\mathbf{R}^* & -i\mathbf{C}_\mathbf{P}^* \\ i\mathbf{C}_\mathbf{R}^\dagger & -i\mathbf{C}_\mathbf{R}^\mathbf{T} & \mathbf{C}_{\mathbf{RR}} & -\mathbf{I}+\mathbf{C}_{\mathbf{RP}} \\ i\mathbf{C}_\mathbf{P}^\dagger & -i\mathbf{C}_\mathbf{P}^\mathbf{T} & \mathbf{I}+\mathbf{C}_{\mathbf{PR}} & \mathbf{C}_{\mathbf{PP}} \end{bmatrix} \begin{bmatrix} \dot{\mathbf{z}} \\ \dot{\mathbf{z}}^* \\ \dot{\mathbf{R}} \\ \dot{\mathbf{P}} \end{bmatrix} = \begin{bmatrix} \partial E/\partial \mathbf{z}^* \\ \partial E/\partial \mathbf{z} \\ \partial E/\partial \mathbf{R} \\ \partial E/\partial \mathbf{P} \end{bmatrix}, \tag{1}$$

where the left-hand side has the usual adiabatic coupling terms $\mathbf{C}_{\mathbf{RR}}$ and nonadiabatic coupling terms $\mathbf{C}_\mathbf{R}$ given by

$$(C_{XY})_{ik;jl} = -2\,\mathrm{Im}\left.\frac{\partial^2 \ln S}{\partial X_{ik}\partial Y_{jl}}\right|_{R'=R,P'=P},$$

$$(C_X)_{ph;ik} = \left.\frac{\partial^2 \ln S}{\partial z_{ph}^*\partial X_{ik}}\right|_{R'=R,P'=P},$$

$$C_{ph;qg} = \left.\frac{\partial^2 \ln S}{\partial z_{ph}^*\partial z_{qg}}\right|_{R'=R,P'=P}. \tag{2}$$

Here, $S=\langle z',R',P'|P,R,z\rangle$ is the overlap matrix. The total energy of the system is

$$E=\sum_k \frac{P_k^2}{2M_k}+\frac{\langle z,R,P|H_{\mathrm{el}}|P,R,z\rangle}{\langle z,R,P|P,R,z\rangle}, \tag{3}$$

with H_{el} the electronic Hamiltonian, which includes the nuclear-nuclear repulsion terms. The system dynamics is treated in a Cartesian laboratory frame, and thus includes the overall translational and rotational degrees of freedom.

Integration of the system yields trajectories of classical nuclei "dressed" with electron-nuclear dynamics. Strictly speaking, the END method is a random-phase approximation [9] approach due to the Thouless determinant, thus it accounts for a small amount of electronic correlation between the same spin electrons. This minimal representation does not account for full electronic correlation and it is implemented into the ENDYNE program package [10].

To analyze the electronic state of the system after the collision, a projection of the single determinantal wave function on various subspaces of electronic wave functions is performed. That is, one obtains the probability P_{if} for a transition from the initial state i to the final state f of the system.

TABLE I. Gaussian basis-set orbital exponents for Ar and H atoms used in these calculations in the END approach.

	Ar		H	
i	α_s	α_p	α_s	α_p
1	674.446518	45.164244	33.870000	1.407000
2	122.851275	10.495199	5.095000	0.388000
3	45.164244	3.413364	1.159000	0.102000
4	33.248349	2.621367	0.325800	0.029064
5	10.495199	0.731355	0.102700	0.008281
6	3.413364	0.286247	0.025260	0.002360
7	2.621367		0.005984	
8	0.731355		0.001417	
9	0.286247			

In order to compute the projected wave function, we transform the orbitals to a basis of energy optimized orbitals for the projectile/target and compute the overlap of the evolving state with all states that can be built in that basis. Due to the choice of basis, the expansion converges quickly, although the projection is computationally expensive. As a consequence of a rearrangement of the Thouless coefficients in Eq. (1) when the differential equations become stiff [9] during the time evolution, a phase factor in the probability amplitude cannot be obtained as a function of the impact parameter (see below).

END calculation approach. The argon target is placed at the origin of the Cartesian laboratory coordinate system and the proton projectile is placed at a distance of $z=30$ a.u. beyond the target on the z axis. The dynamics is stopped when the projectile has passed 30 a.u. from the target or until there is no further change in the charge-transfer probability due to interactions of the projectile and target electronic cloud. For this multielectron system, 30 a.u. of separation is enough to reach convergence within 1% and maintain a computationally feasible calculation.

A proper choice of basis set is crucial in this method. We use Gaussian basis sets of the form

$$\varphi_i(\mathbf{r})=\sum_j d_{ij}(x-R_x)^n(y-R_y)^m(z-R_z)^l e^{-\alpha_j(\mathbf{r}-\mathbf{R}_i)^2} \tag{4}$$

centered on the average nuclear positions $\mathbf{R}_i$ with exponents α_j and contraction coefficients d_{ij}. Here, n, m, and l are integer numbers. From this basis set, a LCAO is formed which then is used to construct the initial molecular orbitals of the system. For the argon atom, we obtain a self-consistent field ground state for the $1s^22s^22p^63s^23p^6$ configuration by means of a $[6s3p/4s3p]$ basis set from Pople [11], augmented by three s and p even-tempered diffuse orbitals to allow for low-lying excitations of the target. For the projectile, we used a $[6s3p/4s3p]$ basis set from Dunning [12], augmented by two s and three p even-tempered diffuse orbitals to reproduce the low hydrogenic excited states. The basis-set exponents used in our calculations are given in Table I. The orbital energies obtained by these basis sets after solution to the Hartree-Fock equations are provided in Table II. The to-

TABLE II. Orbital energies (a.u.) in the Gaussian (END) basis set as obtained in the Hartree-Fock self-consistent field procedure in ENDYNE.

	H		Ar	
i	E_s	E_p	E_s	E_p
1	−0.4993398		−117.2547375	
2	−0.1239286	−0.1238767	−12.2067812	−9.4432514
3	−0.0557926	−0.0540867	−1.2286009	−0.5408670
4	−0.0289234	0.0416203	1.2053897	1.2240550
5	0.2960047	1.2634885	7.3395523	5.9912826
6			55.5542916	19.8909756

tal energies obtained for these atoms are $E(\mathrm{H})=-0.499\,339$ a.u. and $E(\mathrm{Ar})=-522.113\,404$ a.u.. For hydrogen we noticed a good description of the $1s$ and $2l$ orbital energies, as well as for the K, L, and M shells of the Ar atoms. With this basis set, we obtain nine pseudocontinuum states, two of which are too high to describe properly the ionization channel. These energy levels correspond to the isolated hydrogen and argon atoms and are modified once the molecular wave function of the system is constructed under their interaction to obtain the equations of motion as a function of time (or distance).

A number of END trajectories are run with different impact parameters ranging from 0.0 up to 30 a.u. Three ranges of impact parameter are considered: (i) the close interaction region that goes from 0.0 up to 6.0 a.u. in steps of 0.1 a.u.; (ii) the intermediate region covers the range from 6.0 to 10.0 a.u. in steps of 0.5 a.u.; and (iii) the long-range interaction region covers the impact parameters from 10 to 30 a.u. in steps of 1.0 a.u. For the case of near head-on collisions or where strong oscillations were observed in the electron capture probability, a finer grid was used. This yields trajectories for at least a total of 78 impact parameters per projectile energy. The projectile energies computed are 10, 18, 30, 50, 90, 150, 300, 500, 700, 1000, 1500, 2000, 3000, 5000, 7000, 10 000, 16 000, 25 000, 50 000, and 100 000 eV. Thus, in total, over 1600 trajectories have been run. The probability of electron capture is thus calculated from these trajectories to obtain charge-transfer cross sections.

From the projectile nuclei position and momenta in the END approach, we obtain the deflection function of the collision, $\Theta(b,E_p)=\pm\theta-2\pi n$, i.e., the scattering angle as a function of the projectile impact parameter and projectile incident energy. Here, n is the number of orbits that the projectile performs around the target [13]. In this work, only the case $n=0$ occurs. Information on the character of the collision is obtained from the deflection function. For regions where it is positive, a repulsive interaction plays a role. When it is negative, an attractive interaction is occurring. When $\Theta(b_g,E_p)=0$, a glory effects occurs for an impact parameter b_g, and when $d\Theta(b_r,E_p)/db=0$ a rainbow process is in play at the impact parameter b_r [14]. These two processes are the result of the attractive and repulsive part of the interaction potential between projectile and target and produce divergences in the classical differential cross section. Thus a semiclassical correction is required. To this end, we use the Schiff approximation [15,16], which we briefly summarize.

The state-to-state differential cross sections for transfer from the initial state i to the final state f are obtained from

$$\frac{d\sigma_{if}}{d\Omega}=|f_{if}(\theta)|^2, \tag{5}$$

where $f_{if}(\theta)$ is the semiclassical scattering amplitude given by

$$f_{if}(\theta)=ik\int_0^\infty\{\delta_{if}-A_{if}e^{i2\delta(b)}\}J_0(qb)bdb. \tag{6}$$

Here, k is the initial momentum of the projectile, b is the impact parameter, $q=2k\sin(\theta/2)$ is the momentum transferred during the collision, and $J_0(qb)$ is the zeroth order Bessel function with argument qb. In this particular case, we use $A_{if}(b)=\sqrt{P_{if}(b)}$, i.e., the squared root of the probability for an electronic transition from the initial state i into the final state f. Although Eq. (6) is similar to the eikonal result [17], it is obtained by considering all the terms in the Born series. In the eikonal approach, a dependence with the m quantum number appears. Due to the lack of phase factor, as mentioned before, the magnetic quantum number m (axial symmetry in angle φ) has been neglected and we consider the case $m=0$ only. This approximation, however, allows us to obtain some general conclusions on the trajectory effects on the differential electron capture cross section.

The semiclassical phase shift, $\delta(b)$, of the nuclear interaction, as calculated from the deflection function, is given by the expression

$$\Theta(b)=\frac{2}{k}\frac{d\delta(b)}{db}. \tag{7}$$

The differential cross section for transfer into all available electronic levels is now given as the sum of the state-to-state differential cross sections,

$$\frac{d\sigma_{\mathrm{trans}}}{d\Omega}=\sum_f\frac{d\sigma_{if}}{d\Omega}. \tag{8}$$

The probability for electron transfer is calculated as the sum of the individual state-to-state transition probabilities,

$$P=\sum_f P_{if}. \tag{9}$$

The integral cross section for transfer into a given final state is calculated from the appropriate state-to-state transition probability,

$$\sigma_{if}=\int\frac{d\sigma_{if}}{d\Omega}d\Omega. \tag{10}$$

In the case of interference effects on the projectile trajectories being neglected, the previous equation reduces to

TABLE III. Function parameters for the basis set used in the CC calculations.

	Ar			H		
	α	β	k	α	β	k
s	0.010	1.4	18	0.110	1.5	11
p	0.029	1.3	18	0.061	2.0	11
d	0.065	1.4	16	0.042	2.0	8
f	0.030	1.2	15			

$$\sigma_{if} = 2\pi \int_0^\infty b P_{if} db. \tag{11}$$

The integral cross section for electron transfer is then calculated as the sum over all state-to-state integral cross sections.

B. Coupled-channel model

The CC method is a time-dependent semiclassical two-center one-electron approach, combined with a binomial statistical two-electron model [4,18]. In this semiclassical model, the nuclei follows straight line trajectories while the electron dynamics is described by the Schrödinger equation in which the potential is given in Ref. [4]. The projectile-target distance carries implicitly the time dependence. The potential includes the Coulombic interactions between proton-electron and proton-nucleus, and the electron Ar-core interaction

$$V_{e\mathrm{Ar}^+}(r_A) = -\frac{1}{r_A} - (17 + 3r_A)\frac{e^{-2.15r_A}}{r_A}, \tag{12}$$

where r_A is the distance between the electron and the Ar nucleus.

To solve the Schrödinger equation, the wave function is expanded in atomic orbitals centered at each nucleus,

$$\psi = \sum_{i=1}^{N_{\mathrm{H}}} a_i^{\mathrm{H}}(b,t)\phi_i^{\mathrm{H}}(\mathbf{r}_{\mathrm{H}}) + \sum_{i=1}^{N_{\mathrm{Ar}}} a_i^{\mathrm{Ar}}(b,t)\phi_i^{\mathrm{Ar}}(\mathbf{r}_{\mathrm{Ar}}), \tag{13}$$

in which, $\phi_i^{\mathrm{H,Ar}}$ are the atomic functions and include electron translation factors. The atomic states are obtained by a diagonalization of the corresponding atomic Hamiltonian in an even-tempered basis of the form

$$N_l(\alpha\beta^k)e^{-(\alpha\beta^k)r}r^l Y_{lm}(\hat{r}), \tag{14}$$

where N_l is a normalization constant, and the parameters α, β, and k are determined by fitting the atomic energy levels of each ground-state atom to the experimental values, when the atomic Hamiltonians of the system are diagonalized. Although the parameters of the potential were fixed, adjusting the parameters of the basis set allows the eigenfunctions to simulate the Ar ground-state function, which is not equivalent to the exact solution of the Schrödinger equation with the potential of Eq. (12). The fitting procedure was done by using the minimization subroutine MINUIT [19] from the CERN library. The-larger weights were assigned to energies in Ar corresponding to $n=3$, 4, and 5. These wave-function parameter values are displayed in Table III. The energy values obtained after the diagonalization procedure are shown in Table IV.

CC calculation approach. In previous stages of the CC model [4], the behavior of the total capture cross section separated strongly from the experimental data for energies below 7 keV, while the results from the OPM-DFT calculations showed the same trend to the experimental data. Since the physical models used in Refs. [4,5] are similar, the difference between the results was not expected and motivated us to look for improvements in the calculations.

In this work, the atomic basis used contains the lower five s, four p, and three d states for the H atom, and the states from $3s$ to $14s$, $3p$ to $13p$, $3d$ to $12d$, and $4f$ to $12f$ for the Ar atom. There are nine pseudocontinuum states with positive eigenvalues as shown in Table IV. The change in total cross section when the basis includes the pseudocontinuum states is around 2% less (at 50 keV projectile energy) than when

TABLE IV. Orbital energies (a.u.) in the CC basis set.

i	E_s	E_p	E_d	E_f
		H		
1	−0.5000			
2	−0.1250	−0.1250		
3	−0.05555	−0.05549	−0.05556	
4	−0.03121	−0.03023	−0.03107	
5	0.00223	0.1018	−0.01786	
		Ar		
1	−94.98			
2	−12.68	−11.60		
3	−1.072	−0.5780	−0.05723	
4	−0.1424	−0.09505	−0.03233	−0.03125
5	−0.05998	−0.04552	−0.02066	−0.02000
6	−0.03304	−0.02676	−0.01430	−0.01389
7	−0.02088	−0.01759	−0.01045	−0.01020
8	−0.01429	−0.01234	−0.00214	−0.00780
9	−0.01012	−0.00890	0.02878	−0.00613
10	−0.00715	−0.00632	0.09435	−0.00486
11	−0.00494	−0.00411	0.2076	−0.00387
12	−0.00330	0.02198	0.4272	−0.00311
13	−0.00214	0.1520		
14	0.07063			

they are not considered. This is a consequence of the redistribution of probabilities when other channels are opening up.

By projecting the wave function into the different atomic functions, the Schrödinger equation is transformed into a system of coupled equations for the expansion coefficients a_i appearing in Eq. (13). This system of time-dependent differential equations is solved numerically for each of the 232 trajectories specified by an impact parameter distributed nonuniformly in the range 0.02–25.0 a.u. The calculation is done in the overextended range of −100–100 a.u. of internuclear distances, where the value of the coefficients had already converged for this one-electron system. The projectile energies considered were the following: 1, 2, 3, 4, 5, 6, 7, 10, 11, 14, 15, 17, 20, 33, 50, 75, and 100 keV. Initially the Ar atom was in the ground state and the active electron was in one of its subshells, $3s$, $3p_0$, $3p_1$, and $3p_{-1}$.

Since the formalism describes only one independent electron, to simulate the actual contributions from all the eight outer Ar electrons to a given process, we adopted here a binomial model similar to the one described in Ref. [18]. For one electron initially in the Ar subshell j, the probability P_i^j to be transferred to the ith bound state in H is calculated as the square of the expansion coefficients a_i^{H}. In the statistical model used, the single electron capture probability to the ith state is extracted as

$$\begin{aligned} p_i = {} & 2P_i^{3s}\tilde{P}^{3s}(\tilde{P}^{3p_0})^2(\tilde{P}^{3p_1})^2(\tilde{P}^{3p_{-1}})^2 \\ & + 2P_i^{3p_0}\tilde{P}^{3p_0}(\tilde{P}^{3s})^2(\tilde{P}^{3p_1})^2(\tilde{P}^{3p_{-1}})^2 \\ & + 2P_i^{3p_1}\tilde{P}^{3p_1}(\tilde{P}^{3s})^2(\tilde{P}^{3p_0})^2(\tilde{P}^{3p_{-1}})^2 \\ & + 2P_i^{3p_{-1}}\tilde{P}^{3p_{-1}}(\tilde{P}^{3s})^2(\tilde{P}^{3p_0})^2(\tilde{P}^{3p_1})^2, \end{aligned} \tag{15}$$

where the noncapture probability is defined as $\tilde{P}^j = 1 - \sum_i^{\text{states on H}} P_i^j$. The total capture probability is then $\sum_i^{\text{states on H}} p_i$.

III. RESULTS

A. Electron capture probability

Figure 1 shows the probability for finding the electron captured into the $1s$ orbital of the hydrogen projectile, as a function of the projectile impact parameter and collision energy, summed over all the contributions from the $3s$ and $3p$ Ar shell states, as obtained with the END approach. A maximum at ($b \sim 3$ a.u., $E_p \sim 10$ keV) can be observed. This maximum is in agreement with the maximum of the total electron capture cross section around the 10 keV energy region, as is seen below in Sec. III C. It is interesting to see that the maximum makes a ridge toward the high impact parameter region as the energy diminishes, as well as showing an oscillatory behavior in the low to intermediate impact parameter region.

Figure 2 displays the impact parameter dependence of the total electron capture in the projectile as arising from the $3s$, $3p_0$, and $3p_1$ target shells, obtained by the END and CC approaches summed over all the considered bound states of the hydrogen atom at 5 keV. In the same figure, we compare with the theoretical OPM-DFT [5] results. We note that the largest contribution comes from the $3p_1$ argon, whose atomic orbital is perpendicular to the initial projectile direction of motion in agreement with Ref. [5]. The END results are within a factor of 2 at the highest point in the impact parameter ($b \sim 3.5$ a.u.) with respect to the CC and OPM-DFT approaches, while the CC approach is of the same order when compared to the OPM-DFT. However, the CC results have a maximum at $b \sim 4.2$ a.u. The largest discrepancies in the three approaches is for capture from the $3p_0$, whose atomic

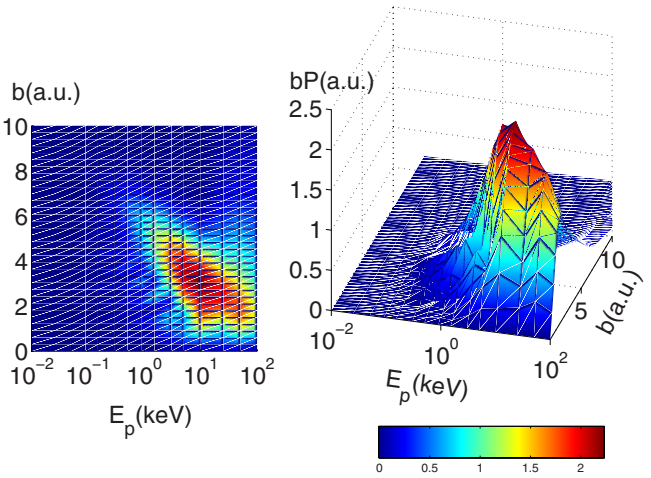

FIG. 1. (Color online) Capture probability into the $1s$ hydrogen orbital for protons colliding with argon atoms as a function of the projectile impact parameter and initial kinetic energy as obtained within the END approach.

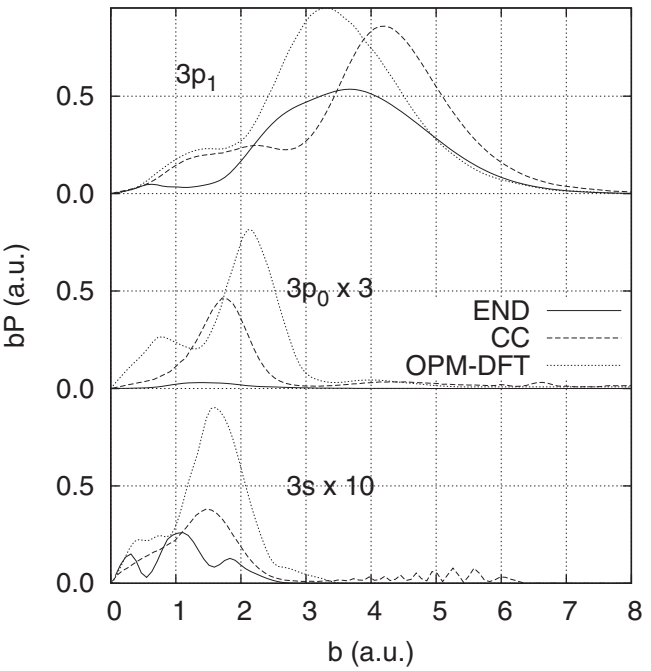

FIG. 2. Impact parameter dependence of the capture probability from the $3s$, $3p_0$, and $3p_1$ states in argon summed over all the available hydrogen states for incident protons at 5 keV. Note the scale factors used in $3s$ and $3p_0$.

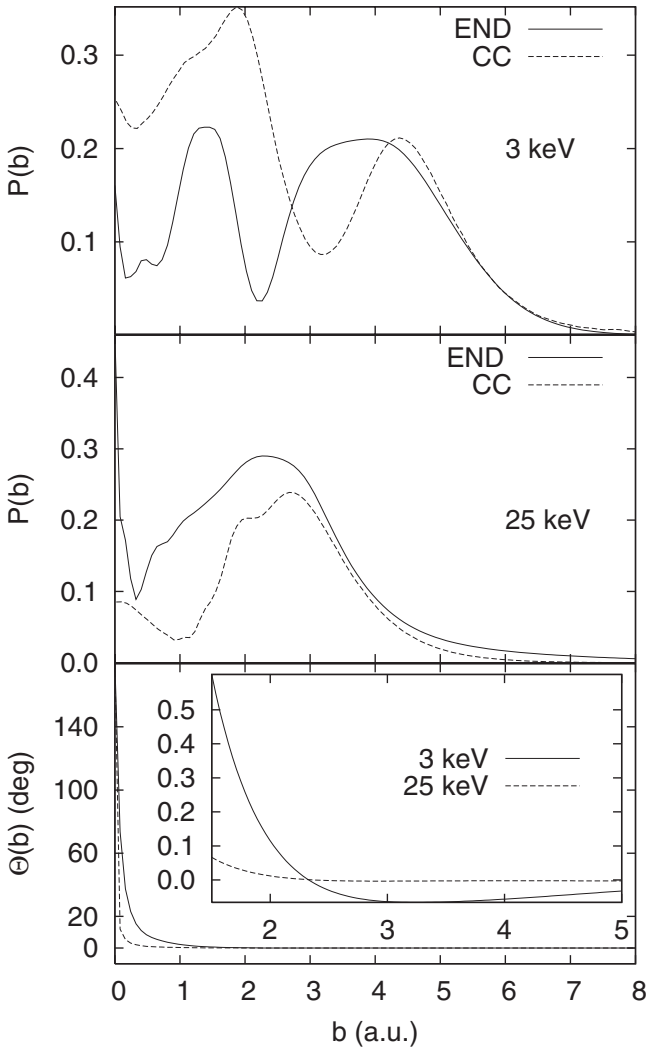

FIG. 3. Impact parameter dependence of the total capture probability for protons colliding on Ar atoms at 3 and 25 keV. The inset shows the deflection function (scattering angle) as a function of the impact parameter for these two energies. See text for discussion.

orbital is aligned with the initial direction of motion of the projectile z axis. Here the CC and OPM-DFT results are within a factor of 2, while the END results are one order of magnitude lower. This striking difference seems to be the result of the straight line trajectory approximation in the CC and OPM-DFT approaches where projectile angular momentum is not conserved during the rotation of the system at the collision, thus forcing a larger electron capture probability (see below).

To assess the effect of the straight line trajectory, we show in Fig. 3 the total electron capture probability summed over all active target subshells and all projectile states as a function of the impact parameter for 3 and 25 keV collision energy as obtained in the CC and END approach. For impact parameters $b>4$ a.u., both approaches are in good agreement. For $b<4$ a.u., the discrepancies start to be notorious. In the same figure, we show the deflection function as obtained in the END approach for these two projectile energies. At 25 keV the scattering angle is small for $b>0.5$ a.u., thus the straight line trajectory is a reasonable assumption. However, at 3 keV noticeably projectile deflection angles are observed for impact parameters $b<1$ a.u., thus the straight line assumption is no longer justifiable. Furthermore and more important, Fig. 3 shows that for impact parameters in the range $1<b<5$ a.u. (see the inset), the effect of the attractive and repulsive region of the interaction potential plays an important role in the electron capture. At 3 keV for $2.5<b<\infty$ a.u. the interaction is attractive. At $b\sim2.5$ a.u. the projectile is not deflected (glory angle), and for $b<2.5$ a.u. the projectile is in the repulsive part of the interaction region since it penetrates the electron cloud and sees the repulsive nucleus. These types of dynamics explain the difference in the electron capture probability from a straight line approach to one in which the trajectory effects are taken into account. At 25 keV, the same effects are observed but in a very small proportion. From similar observations at other energies, we conclude that for projectile energies lower that ~10 keV, the effect of the projectile trajectory is important and should be considered to properly describe the dynamics of electron capture due to the repulsive and attractive part of the interaction potential between projectile and target.

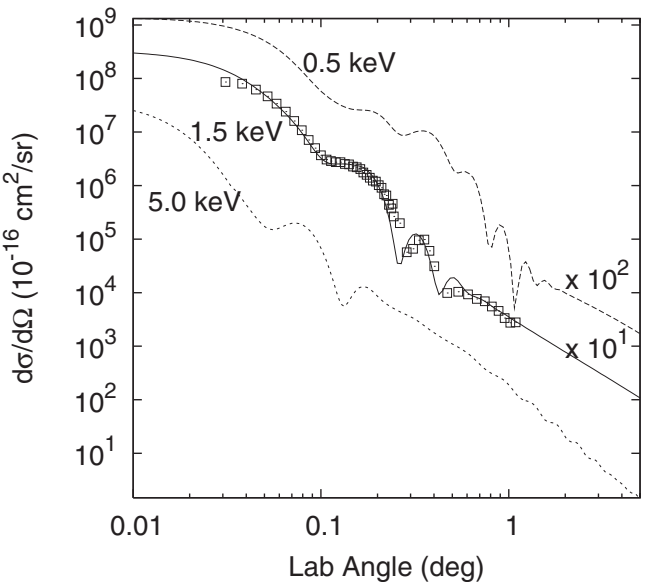

FIG. 4. Direct differential cross section for protons colliding with argon atoms as a function of the scattering angle for projectile energies at 0.5, 1.5, and 5.0 keV as obtained by the END approach. The experimental data are from Johnson *et al.* [20]. Note the scale factors used at 0.5 and 1.5 keV.

B. Direct and charge exchange differential cross section

The process during the collision for which the projectile does not capture electrons but is scattered elastically or inelastically producing excitations and/or ionization in the target is called direct. Figure 4 shows the direct differential cross section for protons colliding with argon atoms as a function of the laboratory scattering angle θ for proton energies of 0.5, 1.5, and 5.0 keV. In the same figure, comparison to the experimental data of Johnson *et al.* [20] for 1.5 keV is provided. An excellent agreement is observed between theory and experiment. This shows that END gives a correct

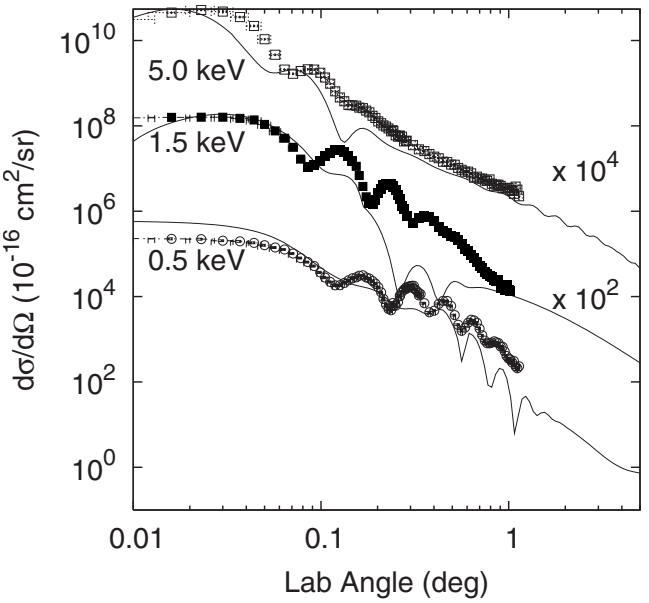

FIG. 5. Charge-exchange differential cross section as a function of the scattering angle for protons colliding with Ar atoms at 0.5, 1.5, and 5.0 keV as obtained by the END approach. The experimental data are from Johnson *et al.* [20]. Note the scale factors used at 1.5 and 5.0 keV.

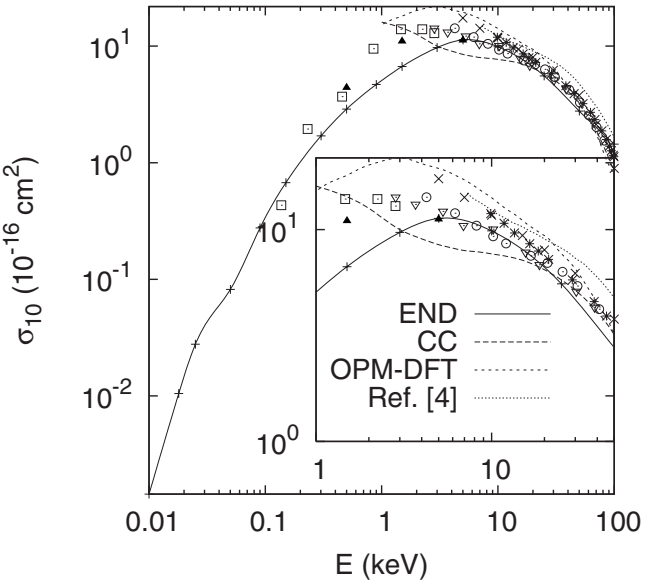

FIG. 6. Total charge-transfer cross section for protons colliding with Ar as a function of the projectile energy. Solid and dashed lines are the results of this work for the END and CC methods, respectively. Short-dash line, OPM-DFT approach [5]. Dotted line, previous CC results [4]. Experimental data: ▲, Johnson *et al.* [20]; □ and ▽, Stedeford and Hasted [21]; ○, Stier and Barnett [22]; ∗, DuBois and Manson [23]; and ×, Rudd *et al.* [24].

description of the scattering process, that is, a proper account of the attractive and repulsive interaction of the collision process. As the energy of the projectile is slowed down, the differential cross section shows more oscillations, characteristic of the interference between the attractive and repulsive trajectories that arise with the same scattering angle (two or more b's that are deflected with the same θ).

From the electron capture probability, one calculates the charge-exchange differential cross section. Figure 5 presents the electron transfer differential cross section for protons colliding at 0.5, 1.5, and 5.0 keV with argon atoms. In the same figure, comparison to the experimental data of Johnson *et al.* [20] is provided. First, one notes that the theoretical results are within a factor of 2 for the 5.0 keV when compared to the corresponding experimental data, although the total cross section for electron capture are almost equal (see the next section). This is due to the optical theorem, which states that $\sigma=4\pi\,\mathrm{Im}\,f(\theta=0)/k$, i.e., the small scattering region gives the larger contribution. The same can be said for the 0.5 keV case. However, for the 1.5 keV the charge-exchange differential cross section for scattering angles between 0.08 and 1 deg is almost two orders of magnitude lower than the experimental counterpart. This is due to interference effects of several trajectories with different impact parameters that scatter with the same angle, thus their probability amplitude overlaps. Since we lack the phase factor in A_{if}, we do not account properly for the interference in this scattering angle. However, the total cross section is within a factor of 2 in this region when compared to the experiment. Work is in progress to obtain a proper description of the probability amplitude phase factor and its effects in the differential capture cross section.

C. Electron capture cross section

Figure 6 shows the total (summed over projectile states) electron capture cross section for protons colliding with atomic Ar as a function of the projectile energy for both CC and END approaches. The obtained results are compared with the experimental data of Johnson *et al.* [20], Stedeford and Hasted [21], Stier *et al.* [22], DuBois and Manson [23], and Rudd *et al.* [24]. In the same figure we show the theoretical data for the OPM-DFT method for comparison [5], as well as the previous CC results [4].

As is observed in Fig. 6, the maximum in the electron capture cross section as a function of the projectile energy corresponds, closely, to the maximum in Fig. 1, since the main contribution to capture comes from the 1s orbital in hydrogen. The END results follow the experimental trend, except for projectile energies between 0.2 and 4 keV, where they are lower than the experimental data. From the previous discussion on the differential cross section, we infer that it is due to interference effects. Furthermore, our results extend below to the unreported region between 0.01 and 1 keV where the cross section has diminished by three orders of magnitude. The improved CC results behave closer to experimental data for the high-energy region, as compared to those previously reported in Ref. [4]. They are also similar to the OPM-DFT curve but separate below 20 keV. The difference between the results of these two approaches may be explained mainly because of the use of different Ar potentials and since the CC eigenenergies for the target do not change during the collision process, while in the OPT-DFT method these energies are adapting dynamically. Another point that we can notice is that the peak shown by the ex-

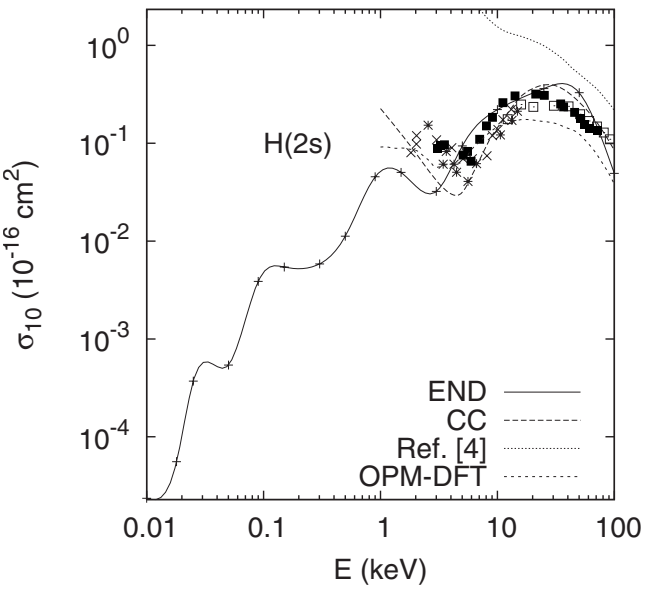

FIG. 7. Electron capture cross section in the $2s$ state of hydrogen for protons colliding with Ar as a function of the projectile energy. The line labels are the same as in Fig. 6. The experimental data are from ∗, [25]; ×, [26]; ■, [27]; □, [28].

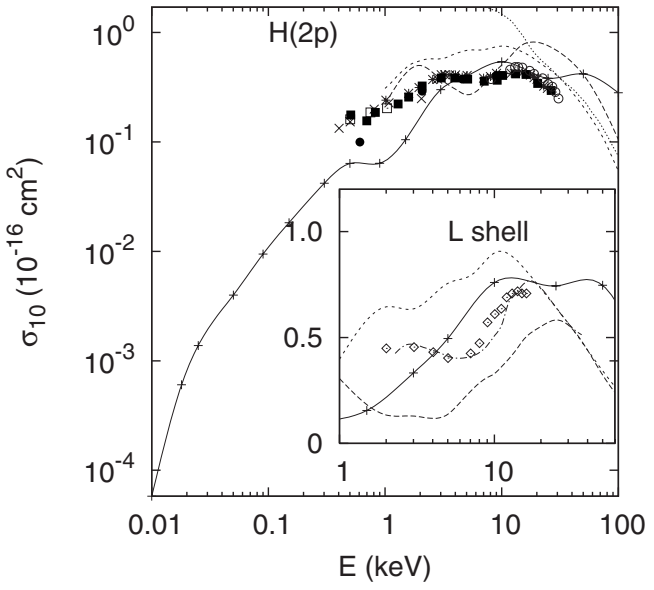

FIG. 8. State-to-state charge-transfer cross section for protons colliding with Ar as a function of the projectile energy. The line labels are the same as in Fig. 6. The experimental data are from ×, [29]; ■, [30]; ∗, [31]; •, [32]; and ○, [33]. Inset: Hydrogen L-shell electron capture cross section (sum over $2s$ and $2p$) as obtained with END (solid line) and CC approaches (dashed line). The OPM-DFT results are shown for comparison (short-dashed line). Experiment: dotted-dashed line obtained by fitting to the experimental data of Ref. [4]; ◇, Risley *et al.* [25].

perimental, OPM-DFT, and END results is not reproduced by the CC approach.

Due to the Coulombic interaction, a Stark mixing occurs in the L and M orbitals in hydrogen, thus a proper diagonalization is required in the projection analysis of the electron capture process for a finite distance of separation between projectile and target. In Ref. [5], the linear Stark mixing was considered. In our case, we have neglected its effects. The scope of this work is focused on comparisons of methods based on the independent-particle model and straight trajectories with those that include multielectronic systems, as well as nonadiabatic effects in the dynamics. We believe that Stark mixing is an important process that needs to be analyzed but goes beyond the purpose of this work. Therefore, we only perform the projection on the isolated eigenfunctions of the projectile (see below).

Figure 7 displays the state-to-state capture cross section into the $2s$ hydrogen orbitals for protons colliding with argon atoms, and comparison to the experimental results of Risley *et al.* [25], Jaecks *et al.* [26], Bayfield [27], and Hughes *et al.* [28] is provided. It is observed that the peak at $E_p \sim 20$ keV is fairly reproduced by the one- and many-electron calculations, as well as the minimum at $E_P \sim 3-5$ keV. At lower energies, the capture cross section is reduced by five orders of magnitude at 10 eV with respect to the maximum at 10 keV as reported by the END approach. One notes that the CC calculations are of the same order as the END, while the OPM-DFT results are a factor of 2 lower in the 10–100 keV region. The END results are higher than the OPM-DFT for projectile energies higher than 4 keV. The OPM-DFT and CC approaches seem to follow a similar trend to END for the low projectile energies considered here. Finally, the END shows a nonmonotonic behavior in the low projectile energy region between 10 eV and 5 keV.

Figure 8 shows the state-to-state electron capture cross section into the $2p$ hydrogen orbitals for protons colliding with argon atoms. Comparison with the experimental results of Van Zyl *et al.* [29], Pretzer *et al.* [30,31], Gaily *et al.* [32], and Andreev *et al.* [33] is also displayed. At lower projectile energies, a descending trend similar to that found in the capture into the $2s$ state, as shown in Fig. 7, is also observed here, although in this case it is monotonic.

In Fig. 8 (inset), we show the sum of the $2s$ and $2p$ states (L shell of hydrogen) and compare with the OPM-DFT since this sum should show no effects from the Stark mixing [5]. We note that the CC and OPM-DFT are very close in the high-energy region. The END is a little higher since it lacks the proper description of the continuum. For projectile energies below 25 keV, the experimental data are between the CC and OPM-DFT theoretical results with the OPM-DFT overshooting the experiment, meanwhile the END are between those two theoretical approaches. The OPM-DFT and CC predict the maximum between 10 and 30 keV as seen in the experimental data.

Since the END basis set lacks a proper description of high angular momentum states, no further comparison for the electron capture into the M or higher shell in hydrogen is provided.

IV. CONCLUSIONS

This work presents differential, total, and state-to-state electron capture cross sections for protons colliding with atomic argon by means of two approaches: a nonadiabatic, fully coupled electron-nuclear dynamics, and a coupled-

channel method. We observe that the main electron capture channel is into the 1*s* state of hydrogen, which exhibits a maximum at $E_p \sim 10$ keV and makes a ridge that extends toward high impact parameter regions and low projectile energies. The results obtained with the END and CC compare fairly well between them and with the OPM-DFT approach for the state-to-state electron capture cross sections and the available experimental data. For projectile energies lower than 10 keV, we find that the attractive and repulsive regions of the interaction potential, which are responsible for the rainbow and glory angle, produce interference effects due to the overlap of two or more trajectories that scatter with the same angle for different impact parameters, thus affecting the electron capture probability. At high projectile energies, the CC approach gives a good description of the electron capture cross section. The same is said of the END approach, although at a higher computational cost. We hope this work will motivate more experimental and theoretical studies for hydrogen beams colliding on atomic argon in the gas phase.

ACKNOWLEDGMENTS

We would like to thank the referee for the comments, suggestions, and for helping us to improve the manuscript. This work was completed with support from PAPIIT Grants No. IN107108 and No. IN105707. We acknowledge the support of the CNS-IPICyT Computing center, as well as Reyes García for the computing help provided at ICF-UNAM.

[1] J. S. Yoon and Y. D. Jung, Phys. Plasmas **6**, 3391 (1999).
[2] W. H. Liu and D. R. Schultz, Astrophys. J. **530**, 500 (2000).
[3] G. Kraft, Prog. Part. Nucl. Phys. **45**, S473 (2000).
[4] A. Amaya-Tapia, H. Martínez, R. Hernández-Lamoneda, and C. D. Lin, Phys. Rev. A **62**, 052718 (2000).
[5] T. Kirchner, M. Horbatsch, M. Keim, and H. J. Lüdde, Phys. Rev. A **69**, 012708 (2004).
[6] J. Kuang and C. D. Lin, J. Phys. B **29**, L889 (1996).
[7] J. Kuang and C. D. Lin, J. Phys. B **29**, 5443 (1996).
[8] D. J. Thouless, Nucl. Phys. **21**, 225 (1960).
[9] E. Deumens, A. Diz, R. Longo, and Y. Öhrn, Rev. Mod. Phys. **66**, 917 (1994).
[10] E. Deumens, T. Helgaker, A. Diz, H. Taylor, J. Oreiro, B. Mogensen, J. A. Morales, M. C. Neto, R. Cabrera-Trujillo, and D. Jacquemin, *ENDyne version 5 Software for Electron Nuclear Dynamics*, Quantum Theory Project, University of Florida, Gainesville, FL, http://www.qtp.ufl.edu/endyne.html (2002).
[11] W. J. Hehre, R. F. Stewart, and J. A. Pople, J. Chem. Phys. **51**, 2657 (1969).
[12] T. H. Dunning, J. Chem. Phys. **90**, 1007 (1989).
[13] D. M. Brink, *Semi-classical Methods in Nucleus-nucleus Scattering* (Cambridge University Press, New York, 1985).
[14] N. F. Mott and H. S. W. Massey, *The Theory of Atomic Collisions* (Clarendon, Oxford, 1965).
[15] L. I. Schiff, Phys. Rev. **103**, 443 (1956).
[16] R. Cabrera-Trujillo, J. R. Sabin, Y. Öhrn, and E. Deumens, Phys. Rev. A **61**, 032719 (2000).
[17] R. McCarroll and A. Salin, J. Phys. B **1**, 163 (1968).
[18] T. Spranger and T. Kirchner, J. Phys. B **37**, 4159 (2004).
[19] F. James and M. Roos, Comput. Phys. Commun. **10**, 343 (1975).
[20] L. K. Johnson, R. S. Gao, C. L. Hakes, K. A. Smith, and R. F. Stebbings, Phys. Rev. A **40**, 4920 (1989).
[21] J. B. H. Stedeford and J. B. Hasted, Proc. R. Soc. London, Ser. A **227**, 466 (1955).
[22] P. M. Stier and C. F. Barnett, Phys. Rev. **103**, 896 (1956).
[23] R. D. DuBois and S. T. Manson, Phys. Rev. A **35**, 2007 (1987).
[24] M. E. Rudd, R. D. DuBois, L. H. Toburen, C. A. Ratcliffe, and T. V. Goffe, Phys. Rev. A **28**, 3244 (1983).
[25] J. S. Risley, F. J. de Heer, and C. B. Kerkdijk, J. Phys. B **11**, 1759 (1978).
[26] D. Jaecks, B. Van Zyl, and R. Geballe, Phys. Rev. **137**, A340 (1965).
[27] J. E. Bayfield, Phys. Rev. **182**, 115 (1969).
[28] R. H. Hughes, E. D. Stokes, S.-S. Choe, and T. J. King, Phys. Rev. A **4**, 1453 (1971).
[29] B. Van Zyl, M. W. Gealy, and H. Neumann, Phys. Rev. A **33**, 2333 (1986).
[30] D. Pretzer, B. Van Zyl, and R. Geballe, in *Proceedings of the Third International Conference on Physics of Electronic and Atomic Collisions* (North-Holland Publishing Company, Amsterdam, 1963), p. 618.
[31] D. Pretzer, B. Van Zyl, and R. Geballe, Phys. Rev. Lett. **10**, 340 (1963).
[32] T. D. Gaily, D. H. Jaecks, and R. Geballe, Phys. Rev. **167**, 81 (1968).
[33] E. P. Andreev, V. A. Ankudinov, and S. V. Bobashev, Zh. Eksp. Teor. Fiz. **50**, 565 (1966). [Sov. Phys. JETP **23**, 375 (1966)].